JACS Au
AN OPEN ACCESS JOURNAL OF THE AMERICAN CHEMICAL SOCIETY

pubs.acs.org/jacsau

Article

Enantioselective Catalysis with Pyrrolidinyl Gold(I) Complexes: DFT and NEST Analysis of the Chiral Binding Pocket

Giuseppe Zuccarello,[§] Leonardo J. Nannini,[§] Ana Arroyo-Bondía,[§] Nicolás Fincias, Isabel Arranz, Alba H. Pérez-Jimeno, Matthias Peeters, Inmaculada Martín-Torres, Anna Sadurní, Víctor García-Vázquez, Yufei Wang, Mariia S. Kirillova, Marc Montesinos-Magraner, Ulysse Caniparoli, Gonzalo D. Núñez, Feliu Maseras, Maria Besora,* Imma Escofet,* and Antonio M. Echavarren*

Cite This: *JACS Au* 2023, 3, 1742−1754

Read Online

ACCESS | Metrics & More | Article Recommendations | Supporting Information

ABSTRACT: A new generation of chiral gold(I) catalysts based on variations of complexes with JohnPhos-type ligands with a remote C_2-symmetric 2,5-diarylpyrrolidine have been synthesized with different substitutions at the top and bottom aryl rings: from replacing the phosphine by a *N*-heterocyclic carbene (NHC) to increasing the steric hindrance with bis- or tris-biphenylphosphine scaffolds, or by directly attaching the C_2-chiral pyrrolidine in the ortho-position of the dialkylphenyl phosphine. The new chiral gold(I) catalysts have been tested in the intramolecular [4+2] cycloaddition of arylalkynes with alkenes and in the atroposelective synthesis of 2-arylindoles. Interestingly, simpler catalysts with the C_2-chiral pyrrolidine in the ortho-position of the dialkylphenyl phosphine led to the formation of opposite enantiomers. The chiral binding pockets of the new catalysts have been analyzed by DFT calculations. As revealed by non-covalent interaction plots, attractive non-covalent interactions between substrates and catalysts direct specific enantioselective folding. Furthermore, we have introduced the open-source tool NEST, specifically designed to account for steric effects in cylindrical-shaped complexes, which allows predicting experimental enantioselectivities in our systems.

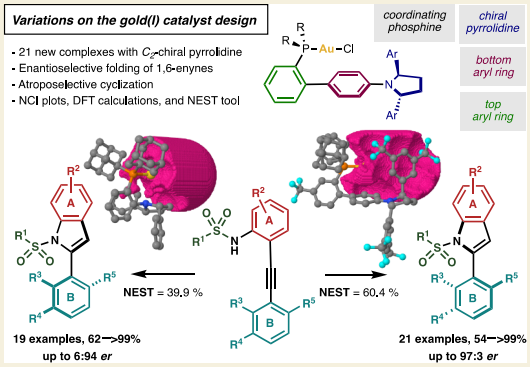

KEYWORDS: *enantioselective catalysis, gold catalysis, enynes, atroposelective cyclization, DFT calculations, NEST tool*

INTRODUCTION

Homogeneous gold(I) catalysis allows for the highly selective activation of alkynes and other multiple C−C bonds, leading to the atom economic construction of complex molecular settings.[1−12] However, the linear coordination of gold(I) complexes, the very low rotational barrier around the gold(I)-unsaturated substrate bond, and the outer-sphere mechanism of the reactions between alkynes and alkenes make the development of enantioselective processes particularly challenging.[13−19] Along with these limitations, some early reports on enantioselective gold(I)-catalyzed transformations lacked in the assignment of the absolute configuration of the final products, so that the exact mode of enantioinduction was ambiguous.[20,21] The development of novel enantioselective gold(I)-catalyzed transformations often relies on the time-consuming and serendipity-driven evaluation of numerous reaction conditions, including ligand families and additives. An alternative approach would include the elucidation of the enantioselective folding of the unsaturated substrate in the catalyst chiral binding pocket, leading to its improvement and ultimately to the establishment of optimized chiral gold(I) catalysts with general application in catalysis. In this context, the groups of Sigman and Toste[22] reported a computational and experimental analysis of axially chiral acyclic diaminocarbene-derived digold(I) complexes, identifying H-bonding within the ligand as the key players for high enantioselectivities in tandem [3,3]-sigmatropic rearrangement/[2+2]-cycloaddition of propargylic esters. Similarly, the groups of Fürstner[23] and Slaughter[24] showed evidence for non-covalent gold(I)−π interactions to shape a chiral environment around the reactive center using phosphoramidite and acyclic diaminocarbene ligands for the activation of eneallenes and internal alkynes, respectively. Finally, Gagné[25] attributed the high performance of axially chiral bisphosphines in gold(I) catalysis to secondary π−π stacking between P-bonded 3,5-xylyl substituents to define a chiral cavity in the cyclization of eneallenes. Emerging enantioselective processes rely on new ligand designs that exploit non-covalent interactions (NCIs)

Received: April 1, 2023
Revised: May 10, 2023
Accepted: May 12, 2023
Published: May 26, 2023

ACS Publications

© 2023 The Authors. Published by American Chemical Society

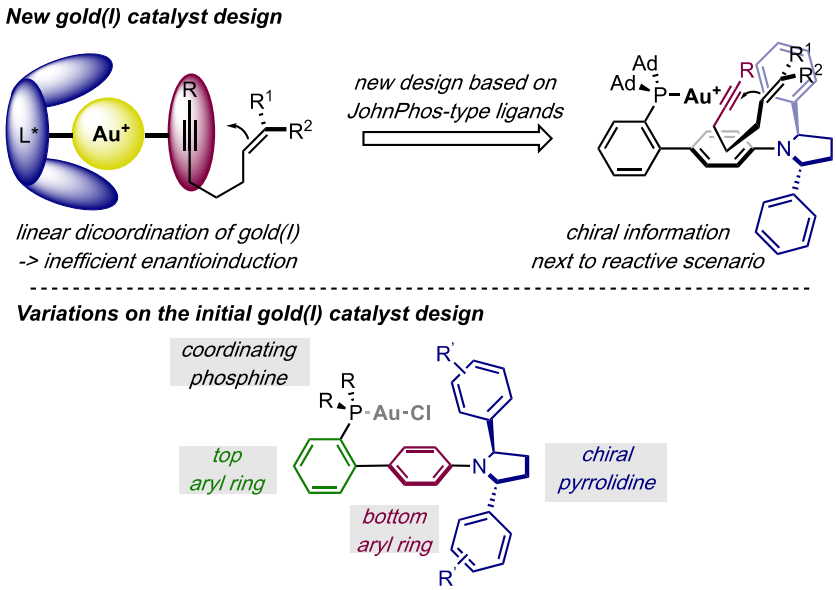

Figure 1. Chiral gold(I) catalysts with a C_2-chiral pyrrolidine and variations on the original design.

within the ligand[26] or with the substrate.[27−32] Analogous approaches were adopted in gold(III)-catalyzed systems with well-defined chiral complexes.[33,34]

As part of our study aimed at understanding the mode of action of chiral gold(I) catalysts,[35] we introduced a family of chiral gold(I) complexes based on JohnPhos-type ligands (Figure 1).[36] This new ligand design features remote C_2-symmetric 2,5-diarylpyrrolidines directly placed at the reaction center, providing high enantioselectivities in three different cyclizations of 1,6-arylenynes, including the formal intramolecular [4+2] cycloaddition of arylalkynes with alkenes[37,38] and other 1,6-enyne cyclizations, such as the synthesis of 1,2-dihydronaphthalenes *via* 6-*endo*-dig cyclization.[36] We proposed a model for enantioinduction based on experimental and computational evidence supporting that the chiral catalysts recognize aromatic groups of the substrates as the stereo directing elements *via* stabilizing NCIs, thus fixing the substrates in the chiral pocket by a preferred binding orientation. This binding mode accounts for the enantioselective folding in the transition state and the observed absolute configuration in the products.

We decided to validate our model by synthesizing a new generation of catalysts based on variations of our original design, modulating steric and electronic properties with different top and bottom aryl rings in the JohnPhos motive, replacing the phosphine by a NHC, increasing the steric hindrance with bis- or tris-biphenylphosphine scaffolds, or by directly attaching the C_2-chiral pyrrolidine at the ortho-position of a dialkylphenyl phosphine. Here, we report the synthesis of new chiral gold(I) complexes and their catalytic activity in the enantioselective intramolecular [4+2] cycloaddition of arylalkynes with alkenes, which we have set as benchmark in the study of our new gold(I) catalysts,[26,36,39] as well as in a new atroposelective synthesis of 2-arylindoles. Extensive DFT computational studies have been carried out to determine the more important attractive interactions between the substrate and the catalyst binding pockets in the possible transition states. Furthermore, a new tool named NEST has been designed to dissect steric ligand effects in cylindrical-shaped complexes and to predict experimental enantioselectivities in our systems.

RESULTS AND DISCUSSION

Benchmarking the New Catalysts in the Intramolecular [4+2] Cycloaddition

New gold(I) catalysts **B**-**W** were tested in the [4+2] cycloaddition of 1,6-enyne **1a** to give adduct **2a** (Scheme 1).[12] Selected data for the cyclization of a similar substrate **1b** are also included.[40] The absolute configuration of adduct (*R*)-**2a** had been assigned before by analogy with that of a related cycloaddition product.[36]

The synthesis of gold(I) chloride complexes **B**-**W** followed procedures analogous to that used for the synthesis of complex **A**, which was the optimal catalyst in our initial study.[12] Thus, for example, the C_2-chiral pyrrolidine in the synthesis of complexes **M**-**O** was carried out from (1*S*,4*S*)-1,4-bis(3,5-bis-(trifluoromethyl)phenyl)butane-1,4-diol **3a**[36] by double mesylation, followed by reaction with *p*-BPin-aniline, to give **4**, which was coupled with 6-bromopicolinaldehyde to form **5** (Scheme 2a). The imines derived from **5** were allowed to react with MOMCl to afford 2,5-disubstituted imidazo[1,5-*a*]pyridin-2-ium chlorides **6a**-**c**, which were converted into gold(I) complexes **M**-**O** by transmetalation of the NHC-Ag(I) intermediates.[41] For the synthesis of **G** and **J**, a cyclic sulfate derived from diols **3** was used instead for the bismesylate in the double S_N2 reaction with the corresponding aniline.[40]

The synthesis of complexes **S**-**W** also commenced with the bismesylation of **3b**-**c** followed by the addition of allylamine to give pyrrolidines **7a**-**b**, which were deallylated under Rh(I) catalysis to afford **8a**-**b** (Scheme 2b). After *N*-benzoxylation of **8a**-**b** to give benzoyl pyrrolidin-1-ols (cyclic hydroxylamines) **9a**-**b**, copper-catalyzed Chan-Lam type coupling with *o*-bromophenyl boronic esters under the conditions developed by Lalic[42] gave **10a**-**b**, which reacted with R_2PH (R = *t*Bu or adamantyl) under palladium catalysis, followed by the addition of $Me_2S{\cdot}AuCl$, to provide gold(I) complexes **S**-**W**.[40] The pyrrolidine of complex **L** was also introduced by copper-catalyzed Chan-Lam type coupling.

New variations **B**-**F** of the original complex **A**[36] led to (*R*)-**2a** with similar enantioselectivities (91:9 to 94:6 *er*), although the [4+2] cycloaddition reactions were significantly faster with catalysts **B** and **D**, bearing one or two CF_3 groups at the

https://doi.org/10.1021/jacsau.3c00159
JACS Au 2023, 3, 1742−1754

Scheme 1. New Gold(I) Catalysts B-W in the [4+2] Cycloaddition of 1a-b[a]

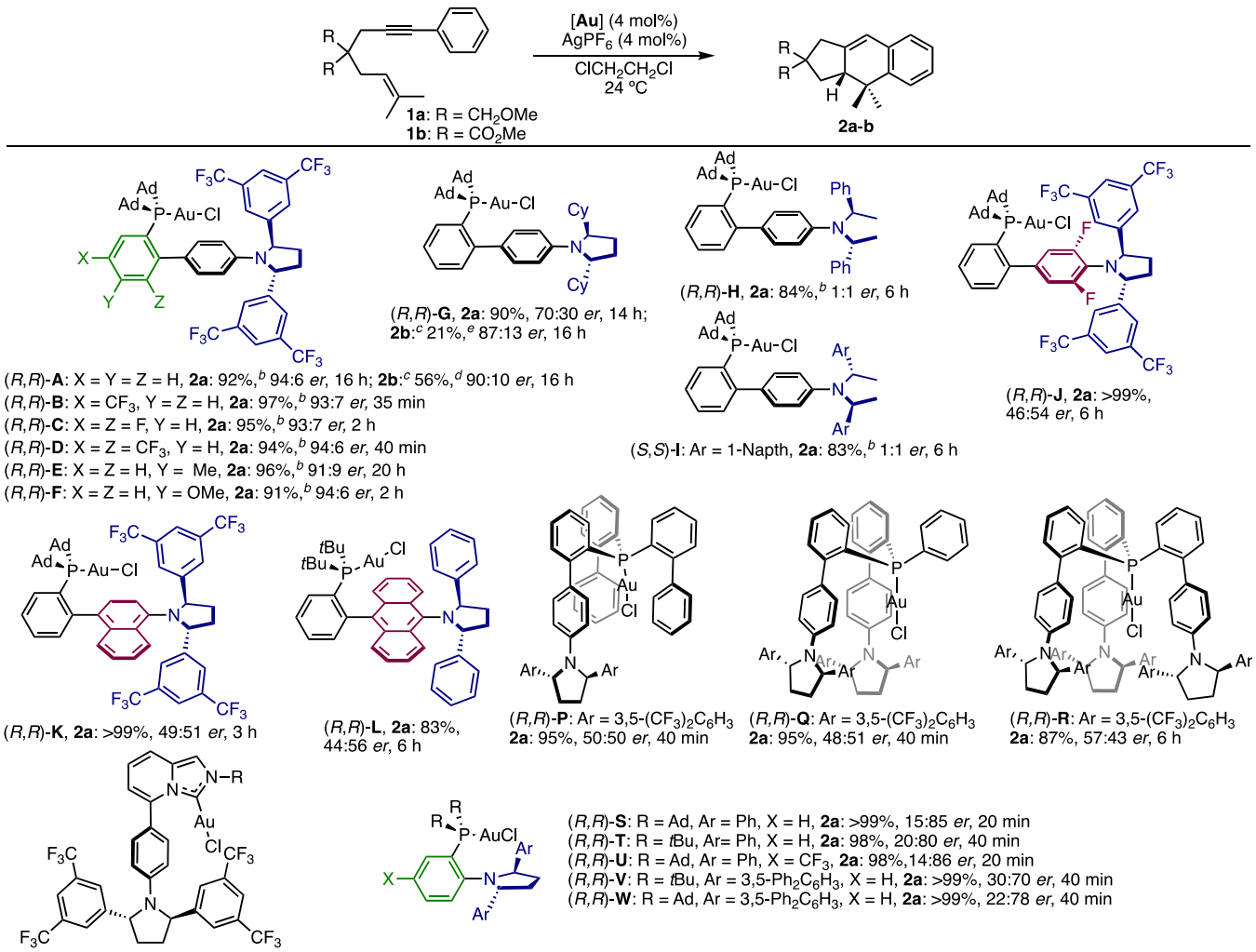

[a]Unless otherwise stated, yields were determined by ^{1}H NMR against internal standard. Enantiomeric ratios were measured by HPLC or supercritical fluid chromatography (SFC). [b]Isolated yield. [c]4 mol % of $AgNTf_2$. [d]68% conversion. [e]41% brsm.

phosphine aryl ring, respectively (Scheme 1). Replacing the aryl groups at 2,5-position of the pyrrolidine by cyclohexyl groups in complex **G** led to lower enantioselectivity (70:30 *er*), whereas complexes **H** and **I** with different C_2-chiral secondary acyclic amines instead of pyrrolidines gave racemic **2a**. Catalysts **J**-**L**, in which the phenyl ring of the biphenyl scaffold has been replaced by 3′,5′-difluorophenyl, 1-naphtyl, or 9-anthracenyl groups gave **2a** in good to excellent yields, although with poor enantioselectivities.

Complexes **M**-**O**, in which the phosphine of **A** has been replaced by an NHC ligand, behave similarly to catalysts **A**-**F**, leading to adduct **2a** in slightly lower enantioselectivities (87:13−89:11 *er*) (Scheme 1). On the other hand, seemingly bulkier complexes **P**-**R** with one, two, or three pyrrolidinylbiphenyl groups at the phosphine led to racemic or nearly racemic **2a**.[43−45] This somewhat surprising result can be ascribed to the deceptively relative high flexibility of these complexes (see later). Remarkably, complexes (*R*,*R*)-**S**-**W** with the C_2-chiral pyrrolidine directly attached to the ortho-position of an aryl dialkyl phosphine led preferentially to the formation of (*S*)-**2a**, which is the opposite enantiomer to that obtained with similarly (*R*,*R*)-configured complexes **A**-**F** and **M**-**O**.

Atroposelective Synthesis of Indoles

Since our first-generation chiral gold(I) catalysts were shown to recognize aromatic groups as the stereo directing elements, we decided to try the atroposelective cyclization of diarylacetylene **11a** to give 2-arylindole **12a** with the second-generation catalysts (Table 1). Chiral biaryl scaffolds are important motifs in privileged chiral ligands,[46−48] organocatalysts,[49−51] biological active natural products,[52−57] and functional materials.[58−61] Enantioselective gold(I) catalysis has recently been shown useful for the synthesis of axially chiral biaryls.[62] Heterobiaryls containing an indole framework are emerging as privileged motifs present in ligands and natural products.[63] An organocatalytic synthesis of axially chiral naphthyl-C_2-indoles *via* cyclization of *ortho*-alkynoanilines using a quinine-derived thiourea catalyst has been reported.[64] More recently, the Pd-catalyzed Cacchi reaction[65] and a chiral silver phosphate-catalyzed cyclization[66] have been used for the atroposelective synthesis of 2-arylindoles.

https://doi.org/10.1021/jacsau.3c00159
JACS Au 2023, 3, 1742−1754

Scheme 2. Synthesis of Chiral Gold(I) Complexes M-O (a) and S-W (b)

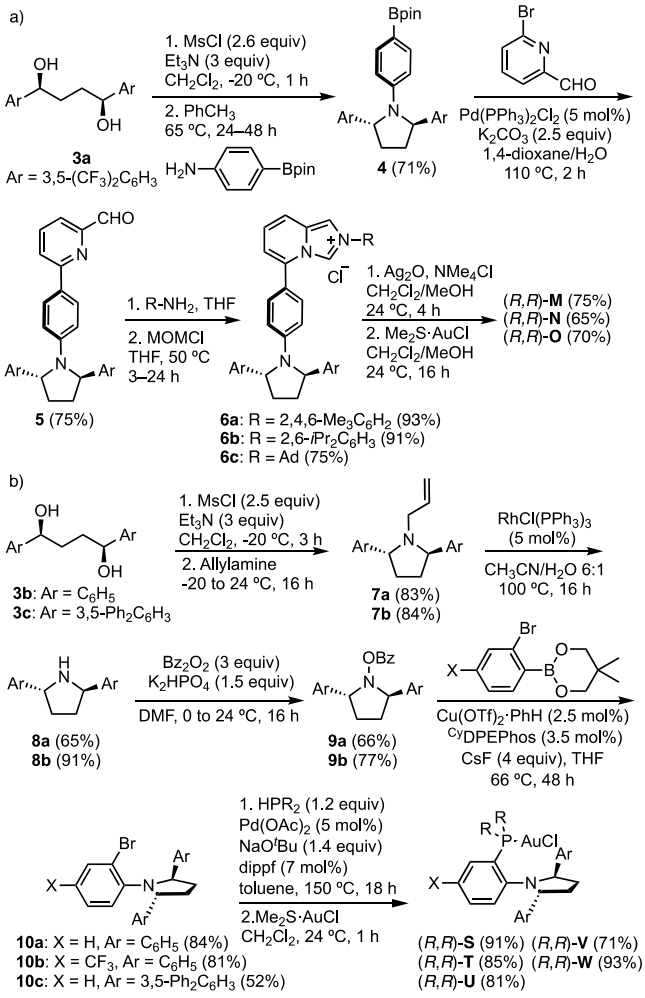

Our study commenced by testing selected chiral gold(I) complexes based on variations of our original design (Figure 1) in the cyclization of sulfonamide **11a** to give 2-arylindole **12a** (Table 1). Initial screening of silver salts showed that $AgNTf_2$ was optimal for the reaction.[40] On the other hand, the solvent showed only little impact on the enantioselectivity of the reaction.[40] However, as observed in other gold(I)-catalyzed reactions, a more coordinating solvent slowed down the catalysis in the following order: 1,2-dichloroethane ≈ CH_2Cl_2 > $PhCF_3$ > PhCl > PhMe > EtOAc. Complex **A**, activated with $AgNTf_2$, led to the clean conversion of **11a** into 2-arylindole (*R*)-**12a** in an excellent yield and 71:29 *er* (Table 1, entry 1). Better enantioselectivity was observed with complex **B**, particularly when the reaction was performed at −4 °C (Table 1, entries 2 and 3). Essentially, the same results were obtained using preformed gold(I) triflimide complex **B′** (Table 1, entries 4 and 5). Lower enantioselectivities were achieved with complexes **G**, **J**, and **L**-**O** (Table 1, entries 6−11). On the other hand, complexes **P**-**R** led to nearly racemic **12a** with a reactivity that significantly decreases with the increase in the steric bulk of the ligand (Table 1, entries 12−14). As found in the [4+2] cyclization of 1,6-arylenynes **1a**-**b**, catalyst (*R*,*R*)-**S** led to the formation of the opposite enantiomer, (*S*)-**12a** (Table 1, entry 15). In this case, good enantioselectivities were obtained when the cyclization was performed at a low temperature (between −4

Table 1. Atroposelective Cyclization of 11a to Form Indole 12a with Chiral Gold(I) Complexes

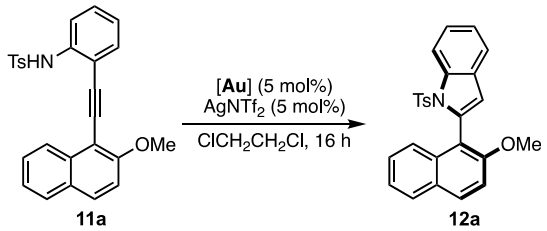

entry	Au catalyst	*T* (°C)	yield (%)[a]	*er*[b]
1	**A**	24	>99	71:29
2	**B**	24	>99	88:12
3	**B**	−4	>99	91:9
4	**B′**	24	91	87:13
5	**B′**	−4	81	92:8
6	**G**	24	96	70:30
7	**J**	24	>99	73:23
8	**L**	24	71	55:45
9	**M**	24	96	67:33
10	**N**	24	97	73:27
11	**O**	24	97	69:31
12	**P**	24	>99	51:48
13	**Q**	24	65	52:48
14	**R**	24	9	[c]
15	**S**	24	>99	15:85
16[d]	**S′**	−4	>99	8:92
17[d]	**S′**	−20	>99	6:94
18[e]	**S′**	−40	>99	5:95
19	**T**	24	>99	27:73
20	**U**	24	>99	15:85
21	**V**	24	>99	68:32
22	**W**	24	>99	71:29
23	[f]	19	91	50:50

[a]Determined by ^{1}H NMR against internal standard. [b]Determined by SFC on chiral stationary phase. [c]Not determined. [d]$PhCF_3$ as the solvent. [e]Toluene as the solvent. [f]Reaction performed with $AgNTf_2$ as the catalyst.

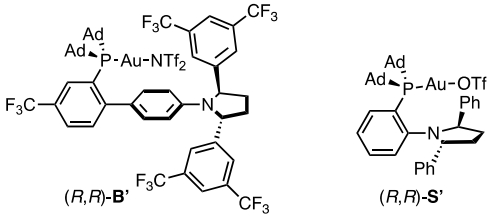

and −40 °C) using a preformed triflate complex (*R*,*R*)-**S′** (Table 1, entries 16−18). Complexes (*R*,*R*)-**T** and (*R*,*R*)-**U** also gave (*S*)-**12a** as the major enantiomer (Table 1, entries 19 and 20), whereas, surprisingly, similar complexes (*R*,*R*)-**V** and (*R*,*R*)-**W**, with terphenyl groups at the pyrrolidine instead of phenyls, led preferentially to (*R*)-**12a** (Table 1, entries 21 and 22). In this system, it is important to note that $AgNTf_2$, used in most cases to generate *in situ* the active gold(I) catalyst, is also, by itself, an active catalyst for the formation of **12a** (Table 1, entry 23).

The scope of the atroposelective synthesis was examined with substituted diarylacetylenes **11a**−**u** with different sulfonamide groups using the optimal two catalysts **B** and **S′**, which allow accessing enantiodivergently (*R*)- or (*S*)-2-arylindoles **12**, respectively (Scheme 3). The absolute configuration of all products was based on those of (*R*)-**12a** and (*R*)-**12l**, whose configuration was assigned by X-ray diffraction, as well as by

https://doi.org/10.1021/jacsau.3c00159
JACS Au 2023, 3, 1742−1754

Scheme 3. Enantiodivergent Atroposelective Cyclization of Diarylacetylenes 11a−u to Form 2-Arylindoles 12a−u with Chiral Gold Catalyst B or S′

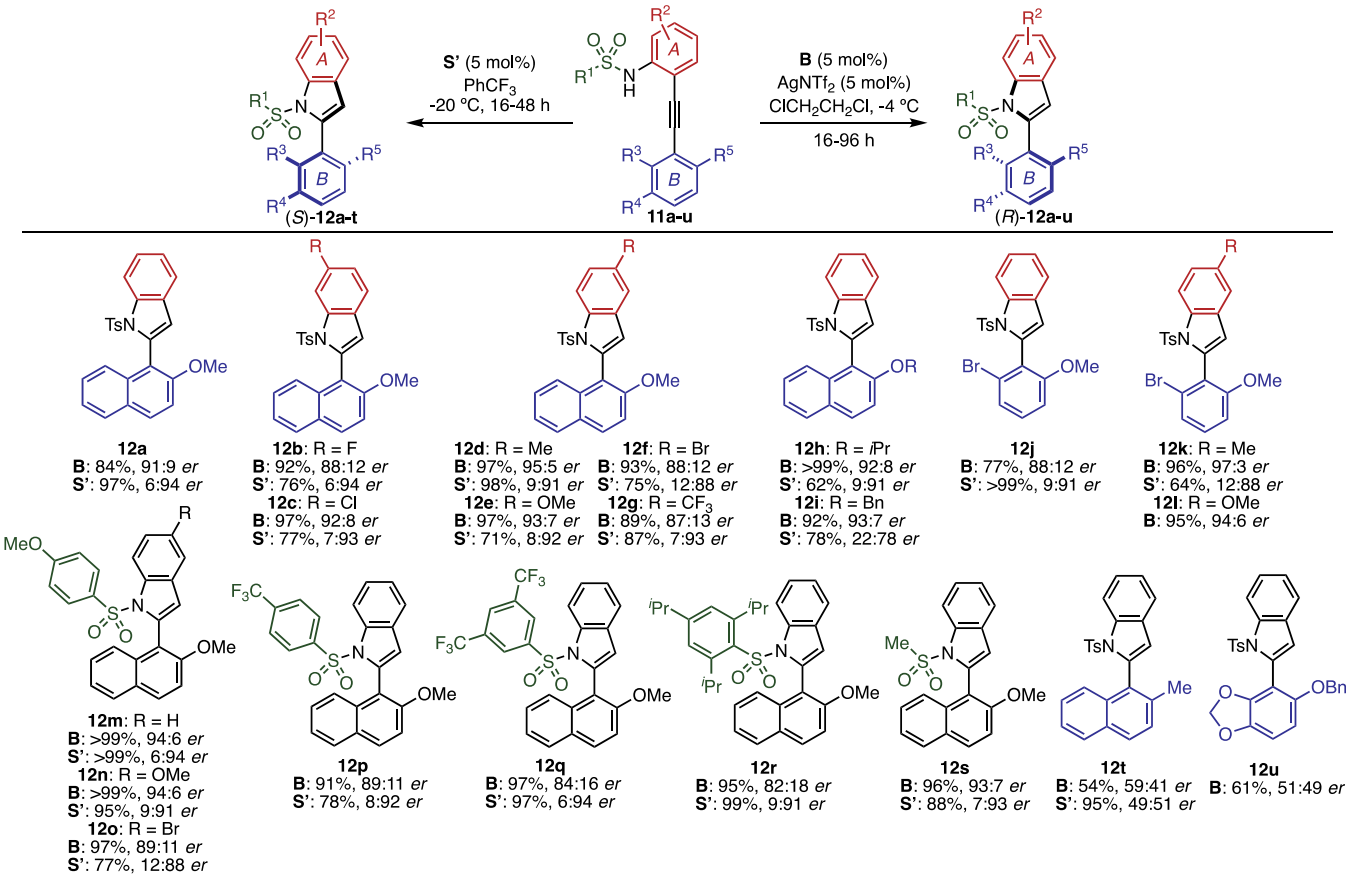

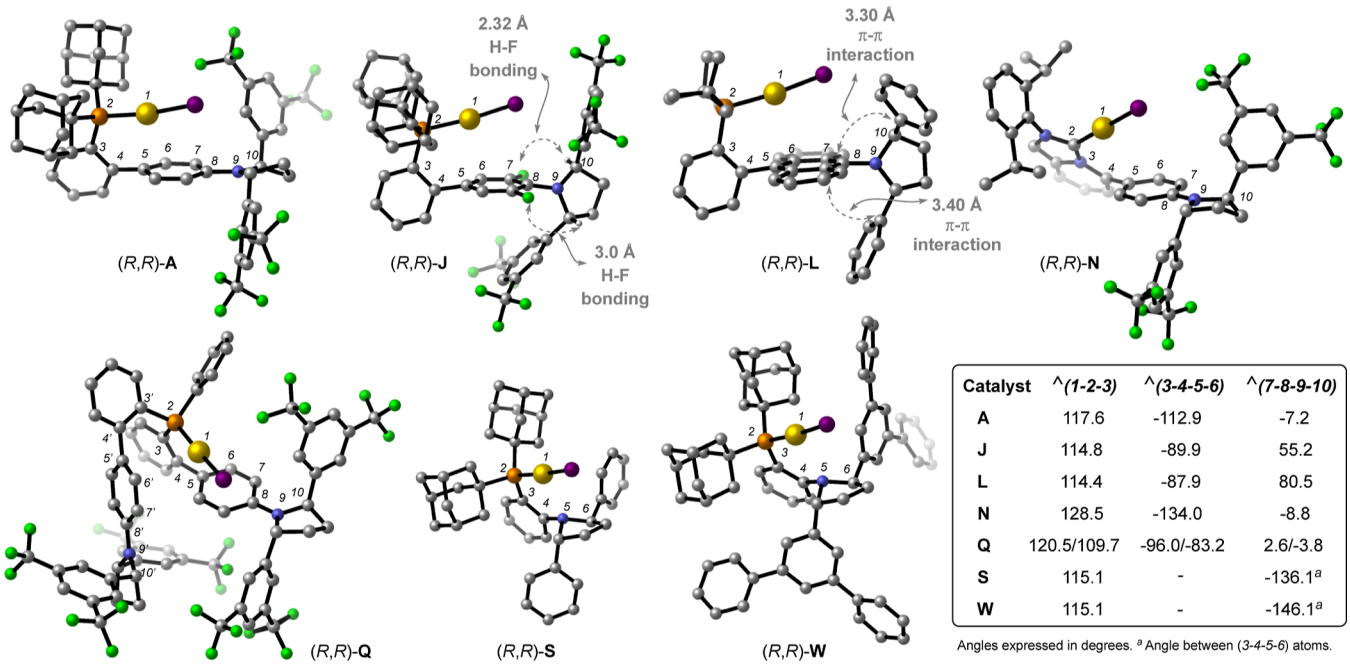

Catalyst	^(1-2-3)	^(3-4-5-6)	^(7-8-9-10)
A	117.6	-112.9	-7.2
J	114.8	-89.9	55.2
L	114.4	-87.9	80.5
N	128.5	-134.0	-8.8
Q	120.5/109.7	-96.0/-83.2	2.6/-3.8
S	115.1	-	-136.1[a]
W	115.1	-	-146.1[a]

Angles expressed in degrees. [a] Angle between (3-4-5-6) atoms.

Figure 2. Selected X-ray crystal structures of complexes **J**, **L**, **N**, **Q**, **S**, and **W** compared with previously related complex **A**. Hydrogen atoms are omitted for clarity.

comparison of the optical rotation of the enantioenriched arylindoles with the literature data.[66] Moderate to good enantioselectivities were observed in all cases, with the exception of **12t** and **12u**, which were obtained as nearly racemic mixtures, most probably due to the lower size of 2-methylnaphthalene in **12t** and benzo[*d*][1,3]dioxole in **12u**.

https://doi.org/10.1021/jacsau.3c00159
JACS Au 2023, 3, 1742−1754

Scheme 4. (a,b) Lowest Energy Intermediates and Transition States of Enyne 1a Coordinated to Catalysts G′ and T, (c,d) Lowest Energy Intermediates and Transition States of Sulfonamide 11a Coordinated to Catalysts B″ and S, 3D Molecular Representations and NCI Plots, (e) CREST Conformational Analysis of Catalysts R and R-Int1 ([LAu(η^2-alkyne)]$^+$ Complex with Enyne 1a)[a]

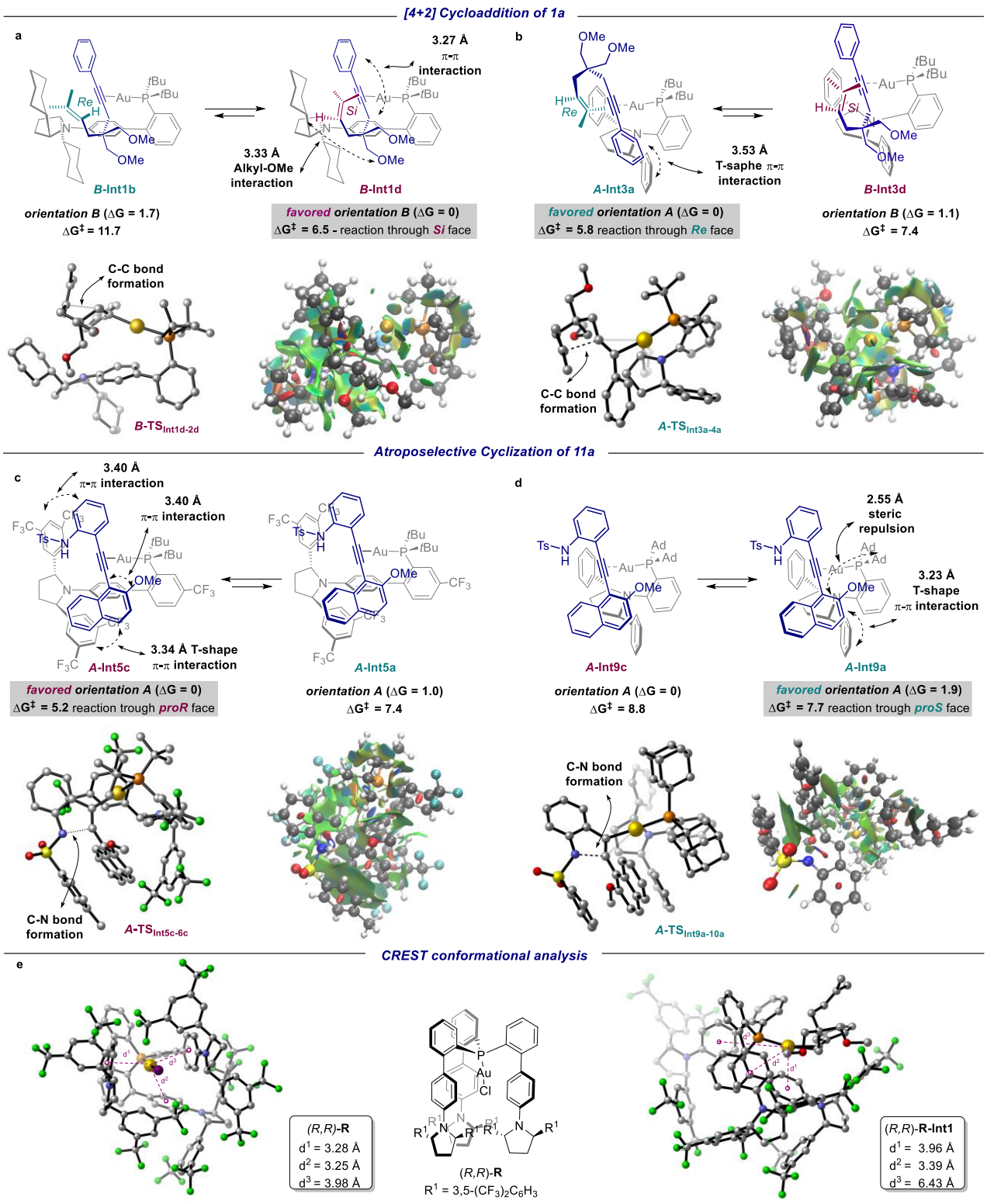

[a]Hydrogen atoms are omitted for clarity. (*S*) Pathways are depicted in cyan and (*R*) pathways in purple. Strong attractive interactions are blue (C−C or C−N bond formation), weak attractive interactions are green (NCIs), and strong repulsive interactions are red. Color code: P: orange, Au: yellow, F: green, N: blue; O: red, C: gray, and H: white. Energy values in kcal/mol relative to the most stable orientation. Calculated bond distances by DFT methods, expressed in Å.

https://doi.org/10.1021/jacsau.3c00159
JACS Au 2023, 3, 1742−1754

Structural Analysis of Chiral Gold(I) Complexes

The structures of new complexes **H**, **J**, **L**, **N**, **P**-**U**, and **W** were confirmed by X-ray diffraction (Figure 2). In solid state, the two aryl groups of the pyrrolidine ring in complexes **N** and **P**-**R** adopt a pseudoaxial/pseudoaxial conformation, similar to that of the parent complex **A**,[36] whereas in **J**, **L**, **S**-**U**, and **W**, the pyrrolidine adopts a conformation with pseudoaxial/pseudoequatorial aryl groups. The bond angle between Au, P, and C3 (atoms 1-2-3, Figure 2) ranges from 114.4 to 117.6° in complexes **A**, **J**, **L**, **P**, **S**-**U**, and **W**, being slightly wider in one of the biaryls of **Q** and **R**. The same angle is much wider in complex **N** with an NHC ligand (128.5°). The pyrrolidine ring in complexes **J** and **L** adopts an approximately perpendicular conformation with respect to the 3′,5′-difluorophenyl or 9-anthracenyl moiety, respectively. The two aryl groups of the biaryl scaffold are almost perpendicular (3-4-5-6 angle, Figure 2) in **J**, **L**, and **Q**, whereas the strongest deviation form perpendicularity occurs in complex **N**.

In the case of **J**, short distances (2.3−3.0 Å) were found between each of the aryl F atoms and the H atoms at C2 and C5 of the pyrrolidine, that are an indication of H−F bonds. On the other hand, in complex **L** the two phenyl groups of the pyrrolidine interact with the anthracene central ring by $\pi-\pi$ stacking with closest contacts of 3.3−3.4 Å.

Computational Study of the Chiral Folding

To rationalize the mode of action of these new chiral catalysts, we studied the cyclizations of enyne **1a** and sulfonamidyl diarylacetylenes **11a** using DFT calculations (BP86-D3/6-31G(d) (C, H, P, O, F, N, S) and SDD (Au), PCM = CH_2Cl_2) with complexes **B**″, **G**′, **S**, and **T** (Scheme 4). Complexes **B**″ and **G**′ are simplified versions of **B** and **G**, respectively, with smaller *t*-Bu instead of adamantyl groups to reduce the computational complexity of the catalyst, without a significant impact on the computed model. Four possible conformations of the gold(I)-enyne **1a** complex were considered: binding orientations *A* and *B* facing, in each case, either the *Re* or the *Si* prochiral face of the alkene, while for **11a**, binding orientations *A* and *B* were considered with either *proR* or *proS* conformation (Scheme 4). Orientation *A* corresponds to that with the arylalkyne (for **1a**) or 2-methoxynaphthyl (for **11a**) closer to the aryl (or cyclohexyl) group at C_2 of the pyrrolidine (more crowded quadrant, see below).

In the cyclization of enyne **1a** with catalyst **G**′, we examined the evolution of the four possible gold(I)-complexes **Int1a**-**d** following an exocyclic pathway. The reaction proceeds from the most stable binding orientation *B* (***B*-Int1d**) through the lowest energy transition state ***B*-TS$_{\mathbf{Int1d\text{-}2d}}$** (favored by 5.2 kcal/mol compared to the lowest *S* pathway, ***B*-TS$_{\mathbf{Int1b\text{-}2b}}$**), to give product **2a** with *R* configuration, by reaction of the alkyne through the *Si* prochiral face of the alkene (Schemes 4a and S1).

On the contrary, using catalyst **T**, enyne **1a** cyclizes *via* orientation *A* (***A*-Int3a**) leading to the *S* enantiomer of substrate **2a**, in accordance with the experimental results (Schemes 4b and S2). In this case, the strong aryl−aryl interaction (T-shape) between the aryl ring of the substrate and the aryl ring of the pyrrolidine in transition state ***A*-TS$_{\mathbf{In3a\text{-}4a}}$** favors the formation of intermediate **A-Int3a** (*S* pathway) by 1.6 kcal/mol. In both cases, the lowest energy transition states were achieved from the most stable orientations (*B* for catalyst **G**′ and *A* for catalyst **T**). NCI plots[67,68] revealed stabilizing alkyl-OMe interactions as stereo-controlling elements that favor the reaction through the *Si* face of the alkene (***B*-TS$_{\mathbf{Int1d\text{-}2d}}$**). Moreover, aryl−alkyl interactions were also observed between the aryl ring of the enyne **1a** and the cyclohexyl ring of the ligand. Recently, alkyl−aryl interactions[69] have been computationally studied by the group of Zarić.[70,71] Based on high-level *ab initio* calculations, this group reported that the most stable stacking for benzene-cyclohexane is 17% stronger than that for benzene−benzene. Nonetheless, as these systems are displaced horizontally, the benzene−benzene interaction retains most of its strength even when displaced at a distance of 5.0 Å, where the benzene−benzene attraction is still ∼70% of its maximum strength, while the benzene-cyclohexane attraction falls to ∼40% of its maximum strength. Therefore, $\pi-\pi$ interactions between aromatic compounds are generally stronger, since they retain the strength of attraction over a larger range. Nevertheless, at short distances, cyclohexane-benzene can form strong electrostatic interactions.

Recognition of substrate **11a** by chiral catalysts **B**″ and **S** was also studied by DFT calculations (Schemes 4c,d and S3−S5). Hence, binding orientation *A* was favored by NCIs and leads to the distinct enantioselective folding in the atroposelective synthesis of indole **12a**. The lowest transition state ***A*-TS$_{\mathbf{Int5c\text{-}6c}}$** is stabilized by NCIs between the sulfonamide **11a** and the chiral pocket of catalyst **B**″. Therefore, the corresponding intermediate ***A*-Int6c** is preferentially formed, leading to product **12a** with the *R* absolute configuration ($\Delta\Delta G^{\ddagger}$ = 2.2 kcal/mol), in good agreement with the experimental results (91:9 *er* with analogue catalyst **B**) (Schemes 4c and S3). For catalyst **S**, the computed energies suggest that the two possible pathways from orientation *A* can compete. Although the intermediate *proR* (***A*-Int9c**) is 1.9 kcal/mol more stable than the intermediate *proS* (***A*-Int9a**) (Schemes 4d and S5), the major product arises from the latter through the *proS* transition state ***A*-TS$_{\mathbf{Int9a\text{-}10a}}$**, which is lower in energy ($\Delta\Delta G^{\ddagger}$ = 1.1 kcal/mol) than ***A*-TS$_{\mathbf{Int9c\text{-}10c}}$** in a Curtin-Hammett scenario. Again, NCI plots illustrate the size and shape of the surfaces generated from interactions present in these systems (Scheme 4c,d). Hence, T-shape $\pi-\pi$ interactions between the naphthyl ring of the substrate and the aromatic substituent of the pyrrolidine play the major role in the chiral folding of sulfonamide **11a** and in the stabilization of the corresponding transition states.

Furthermore, conformational sampling performed with semiempirical CREST based on xTB methods[72] was used to study the complexes **P**, **Q**, and **R** with very large ligands and the corresponding **Int1** ([LAu(η^2-alkyne)]$^+$) complexes with enyne **1a** (Scheme 4e). In each case, the lowest energy conformer was reoptimized at DFT level.[40] The calculated bond distances between the gold atom and the *o*-aryl centroid of each aryl ring shows the unexcepted high flexibility of these systems. Thus, upon the coordination of the enyne to the gold(I) center, the intermediate reorganizes, leading to a wide-open catalytic pocket that places the chiral information provided by the C_2-symmetric pyrrolidines far away from the reaction center reducing drastically the enantioinduction, as observed experimentally in the formation of the nearly racemic product **2a**.

NEST Occupied Volume Analysis

In the key transition states presented above, the calculated distances between gold(I) and the more distant carbon of the new C−C bond are about 5.0 Å (4.962 Å for **B-TS$_{\mathbf{Int1d\text{-}2d}}$**), which suggest that, in addition to steric effects at the proximities of the metal center, effects at longer distances could have a significant impact on the enantioselectivity. To study ligand effects in our gold(I) catalysts, we initially analyzed the structures optimized computationally, based on the X-ray crystal structures, by

https://doi.org/10.1021/jacsau.3c00159
JACS Au 2023, 3, 1742−1754

calculating their Buried Volumes[73] with SambVca,[74] as commonly done in the analysis of gold(I) complexes with bulky ligands.[39,74−76] However, to more properly describe the elongated gold(I) catalysts, we have developed the NEST tool (Figure 3), inspired by SambVca and MolQuo[77,78] tools. The

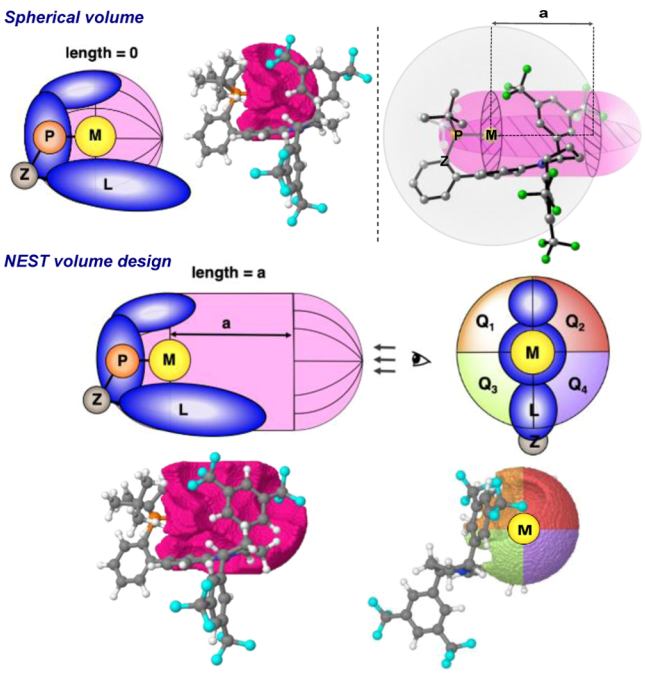

Figure 3. NEST Volume design and example of complex **A′**.

open-source web program NEST has been designed for the evaluation of the steric effects of metal catalysts bearing voluminous ligands that create a non-spherical nest. Although SambVca allows to make the sphere around the metal as large as desired, this sphere would contain large empty spaces that are irrelevant for the description of the reactivity, leveling the differences among the analyzed complexes with diverse bulky ligands.

NEST considers a volume of capsule shape (a cylinder with round ends) and computes the percent volume occupied by the atoms (NEST occupied volume). Dividing the space between the central atom (M) and the end of the capsule in quadrants, NEST also provides the quadrant's occupied volumes $Q1_{occ}$, $Q2_{occ}$, $Q3_{occ}$, and $Q4_{occ}$. The length a can be tuned depending on the system of interest (Figure 3).[40]

Selected data of the NEST occupied volume are shown in Table 2 and Figure 4. In addition, an mp4 file is provided with a representation of NEST occupied volume for all studied complexes.[40] For example, at the cylinder length a = 4 Å, NEST volumes of 61−65% were calculated for complexes **A′**, **B**, and **J**, which are structurally similar to the parent gold(I) catalyst **A** (Table 2, entries 1−3, and 6). It is somewhat surprising how the addition of a CF_3 in meta-position with respect to the phosphine in complex **B**, which is seemingly sterically neutral, leads to a reduction of the occupied volume from 64.8 to 60.4% (compare entries 1 and 3, Table 2). However, the optimized DFT structures of complexes **A** and **B** show significant differences in the conformational minimum: the bond angle between Au, P, and C3 (atoms 1-2-3, see Figure 2 for the numbering) is wider in **B** (120.1°) than in **A** (116.6°) and the biaryl dihedral angles are also different (−62.8° for **B** and −78.0° for **A**).[40] Complex **G** with cyclohexyl instead of aryl groups at the pyrrolidine shows a lower occupied volume of 55% (Table 2, entry 4). Complex **L**, with an almost perpendicular anthracene with respect to the aryl phosphine (Figure 2), has a low NEST occupied volume of 50% (Table 2, entry 7), which is similar to that found in NHC gold(I) complexes **M** and **N** (Table 2, entries 8 and 9), although the distribution of the occupied volume among quadrants Q1-Q4 is very different (Table 2 and Figure 3). As expected, the lowest volumes were found in gold(I) complexes **S**-**U** and **W** (Table 2, entries 10−13). Complexes **S**-**U** show almost identical occupied volumes of 39.4−39.9% (Table 2, entries 10−12), whereas only a modest increase was found for **W** (42.5%), despite the steric difference of the pyrrolidine substituents (terphenyl in **W** *vs* Ph in **S**-**U**).

Table 2. NEST Parameters Used for Selected Gold(I) Catalysts[a]

entry	cat.	NEST	$Q1_{occ}$	$Q2_{occ}$	$Q3_{occ}$	$Q4_{occ}$
1	**A**	64.8	86.0	25.7	88.9	19.1
2	**A′**	61.3	92.7	26.3	72.2	11.8
3	**B**	60.4	79.8	24.5	86.7	16.0
4	**G**	55.0	30.5	15.2	76.2	47.5
5	**H**	47.0	6.4	7.4	66.9	43.0
6	**J**	62.2	80.9	20.0	83.6	21.5
7	**L**	50.0	18.1	7.9	73.4	38.1
8	**M**	48.7	6.7	48.7	16.5	73.3
9	**N**	50.8	10.4	24.9	50.6	60.5
10	**S**	39.9	6.5	7.6	29.3	37.4
11	**T**	39.4	6.8	6.7	29.4	37.1
12	**U**	39.7	6.4	7.4	29.1	37.1
13	**W**	42.5	7.0	21.8	28.6	39.2

[a]NEST occupied volume, $Q1_{occ}$, $Q2_{occ}$, $Q3_{occ}$, and $Q4_{occ}$ expressed in % at cylinder length a = 4 Å. The total length of the capsule is 3.5 + a + 3.5 Å.

With the aim of building a model to reproduce and predict enantiomeric ratios, NEST results for each catalyst were used as descriptors alone or in combinations, *i.e.* occupation of the upper quadrants ($Q1_{occ}$ + $Q2_{occ}$), the lowest ($Q3_{occ}$ + $Q4_{occ}$), or the diagonal ($Q1_{occ}$ + $Q4_{occ}$ or $Q2_{occ}$ + $Q3_{occ}$), among others,[40] in an approach similar to previous works.[79,80] Geometries given to NEST are DFT-optimized structures of the neutral gold(I) chloride complexes obtained by X-ray diffraction. Single variable linear regressions between each descriptor derived from NEST and experimental *er* were evaluated for three substrates (**1a**, **1b**, and **11a**). We first searched the best correlation for the previously reported substrate **1b**[36,81] and found that the experimental *er* has a relationship with descriptor D_1 with an r^2 = 0.97. The equation obtained is $er = 266 - 20{,}492D_1$, D_1 being the inverse of the occupancy of the most occupied pair of quadrants, upper ($Q1_{occ}$ + $Q2_{occ}$) or lower ($Q3_{occ}$ + $Q4_{occ}$) and for length a = 3 Å. In other words, the enantioselectivity is related to the occupancy of the most hindered half moiety of the nest. Increasing the occupancy of the most hindered pair of quadrants (upper or lower), the enantioselectivity increases.

For the cyclization of enyne **1a**, the enantiomeric ratio showed a relationship with several NEST-derived descriptors, being the best D_2, following the equation $er = 158 - 6093D_2$ (r^2 = 0.93). The predicted values according to this equation are presented in Table 3. If complexes **M** and **N**, with a structurally different NHC ligands, and **H**, which does not contain a pyrrolidine were removed from the set, the r^2 coefficient would raise up to 0.99. D_2 is the inverse of the sum of the occupancy of the quadrants

https://doi.org/10.1021/jacsau.3c00159
JACS Au 2023, 3, 1742−1754

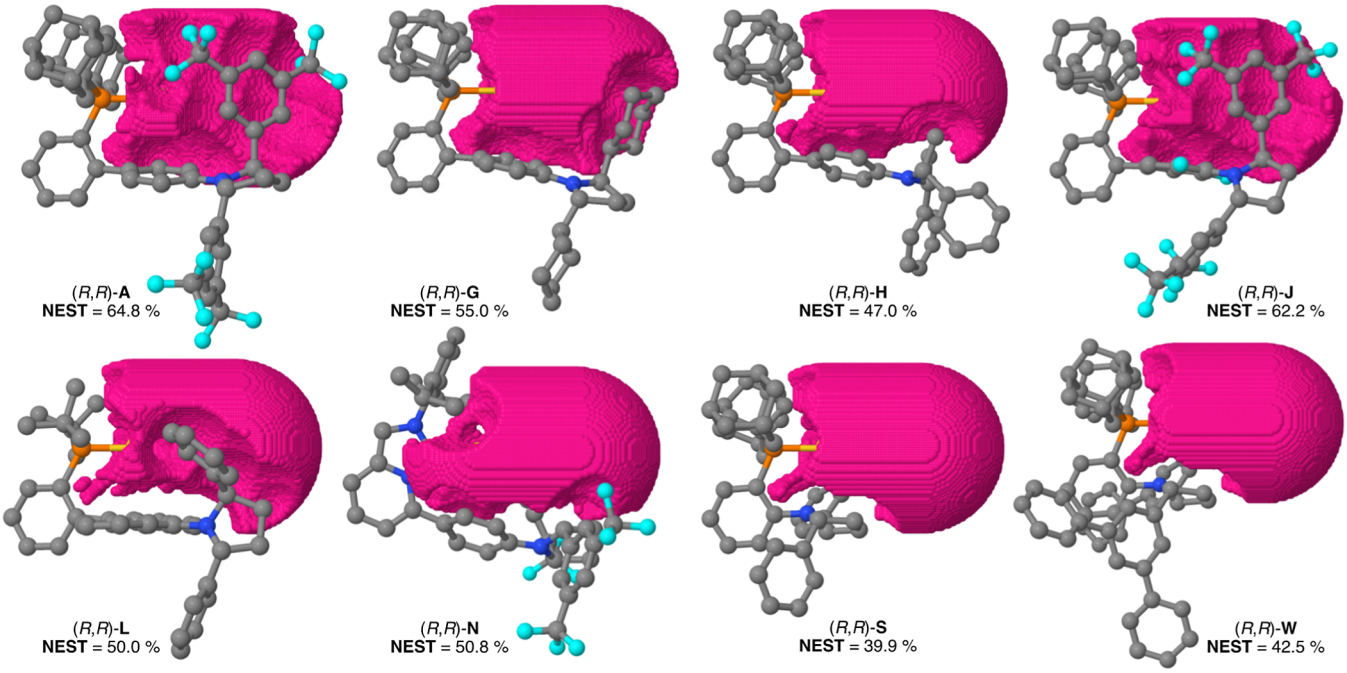

Figure 4. NEST occupied volume of selected gold(I) complexes (a = 4 Å).

Table 3. Calculated (pred) and Experimental (exp) Enantiomeric Ratios for the Formation of 2a and 12a[a]

entry	cat.	2a (pred)[a]	2a (exp)	2b (pred)[b]	2b (exp)	12a (pred)[c]	12a (exp)
1	**A**	100:0	94:6	83:17	90:10	83:17	71:29
2	**A′**	100:0	90:10	86:14	86:14	80:20	71:29
3	**B**	95:5	93:7	74:26		82:18	88:12
4	**G**	80:20	70:30	87:13	87:13	70:30	70:30
5	**H**	35:65	50:50	88:12		21:79	
6	**J**	99:1[d]	46:54	81:19		82:18	73:27
7	**L**	50:50	44:56			54:46	55:45
8	**M**	82:18	89:11	51:49	87:13	74:26	67:33
9	**N**	72:28	88:12	94:16		64:36	73:27
10	**S**	20:80	15:85	7:93	17:83	23:77	15:85
11	**T**	20:80	20:80	6:94		20:80	27:73
12	**U**	18:82	14:86	5:95		21:79	15:85
13	**W**	26:74	22:78	11:89		58:42	71:29

[a]D_2 used as descriptor for the nucleophilic attack in **1a**. $er = 158 - 6093D_2$. [b]D_1 used as descriptor for the nucleophilic attack in **1b**. $er = 266 - 20{,}492D_1$. [c]D_3 used as descriptor for the atroposelective formation of **12a**. $er = 92 - 969D_3$. [d]Outlier removed from the training set presumably due low mobility of the pyrrolidine.

Q1 and Q4 for length a = 4 Å. This descriptor represents the occupancy of two diagonal quadrants, similar to previous case er increases as $Q1_{occ}$ and $Q4_{occ}$ increase, presumably inducing the voluminous parts of the substrate to occupy the other diagonal. These results, together with the study with substrate **1b**, suggest that increasing the occupancy of the ligand in quadrant Q1 at long distances increases the enantioselectivity of both substrates in the [4+2] cycloaddition reaction. Please note that catalyst **J** is an outlier in the group, very likely due to low mobility of the pyrrolidine.[40]

On the other hand, for the atroposelective reaction with substrate **11a**, the enantiomeric ratio shows a relationship with the descriptor D_3, being the inverse of the smallest occupancy of the upper ($Q1_{occ}$ + $Q2_{occ}$) or lower ($Q3_{occ}$ + $Q4_{occ}$) quadrants for length a = 4 Å. D_3 is similar to D_1 (used for substrate **1b**), although better results were obtained with the occupancy of the least hindered moiety. The equation is $er = 92 - 969D_3$ (r^2 = 0.91), and the enantioselectivity also increases with increasing occupancy (Table 3). Again, a slightly better correlation r^2 = 0.95 was found removed from the training set complexes with NHC ligands **M** and **N** and the very substituted **W**. The error of enantiomeric predictions increases for catalyst **S**-**W** (Table 3, entries 10−13) but the stereodivergent atroposelective formation of indoles **12a** (opposite to the other family of complexes) is well reproduced.

Finally, the equations obtained for each substrate and the descriptors obtained from the NEST App can be used to predict enantiomeric ratios of all computationally studied catalysts. So, we can easily apply the catalyst descriptors to all three equations and check if there is any synthetized catalyst with interesting results for a reaction and substrate, not experimentally tested. Predictions were made (see Tables S9−S14)[40] and catalysts **S**, **T**, and **U** showed potentially interesting results for the cyclization of enynes **1b**. Thus, for example, an er of 7:93 was predicted for the formation of (S)-**2b** with catalyst **S**, which was validated with an experimental value of 17:83, within the expected error. A similar error (100:0 *vs* 90:10) was found for the reaction of (R)-**1a** with catalyst **A′**, not included in the training set, supporting in both cases the validity of our models.

CONCLUSIONS

We have explored catalysts space based on variations of gold(I) complexes with a JohnPhos-type scaffold by synthesizing 22 new members of the family, making a total of 29 complexes including the previously reported first-generation catalysts.[36] These chiral gold(I) catalysts have been tested in the intramolecular [4+2] cycloaddition of arylalkynes with alkenes and in the atroposelective synthesis of 2-arylindoles by cyclization of sulfonamidyl diarylacetylenes. Adding an electron-withdrawing CF_3 group at the meta-position of the aryl phosphine of the JohnPhos-type ligand leads to complex **B**, which is a more active

https://doi.org/10.1021/jacsau.3c00159
JACS Au 2023, 3, 1742−1754

catalyst than the parent complex **A**. On the other hand, bulkier bis- or tris-biphenylphosphino ligands or those with the scaffolds that fix the pyrrolidine in an almost perpendicular conformation with respect to the aryl form gold(I) complexes that lead to poor enantioselectivities. Remarkably, gold(I) catalysts with smaller ligands, such as **S**, in which the C_2-chiral pyrrolidine is directly attached at the ortho-position of a dialkylphenyl phosphine, led to the formation of the opposite enantiomers in the [4+2] cycloaddition and the atroposelective synthesis of 2-arylindoles with good enantioselectivities. This allows obtaining both series of products in an enantiodivergent manner using catalysts that have the same absolute configuration at the C_2-chiral pyrrolidine.

Analysis of the chiral binding pockets of the new gold(I) catalysts by DFT calculations shows the importance of stabilizing NCIs in determining the preferred reaction pathway. To study ligand effects in our gold(I) catalysts, bearing voluminous ligands that create a non-spherical nest, we have developed the new open-source tool NEST App, specifically designed to account for steric effects in cylindrical-shaped metal complexes. To evaluate the steric effects of our gold(I) catalysts, as a first approximation, we have used their X-ray crystal structures, which were optimized by DFT calculations. The equations obtained for each substrate and the descriptors obtained from the NEST App were used to predict the enantiomeric excesses, with reasonable agreement with the experimental results in most cases. Although these predictions do not replace more rigorous DFT calculations nor NCI analysis of the chiral pockets, NEST could allow speeding up the design of new chiral catalysts.

METHODS

General Procedure for the Synthesis of Axially Chiral Indoles 12

General Procedure for the Synthesis of (*R*)-Indoles. Ts-protected anilines and (*R*,*R*)-**B** (5 mol %) were dissolved in 1,2-dichloroethane, and the mixture was cooled to −4 °C. A solution of $AgNTf_2$ (5 mol %) in 1,2-dichloroethane (total concentration 0.05 M) was added dropwise, and the reaction was stirred at the same temperature for the given time. After full conversion of the starting material, the reaction was quenched by the addition of 3 drops of Et3N and concentrated. The crude was purified by flash column chromatography or preparative thin-layer chromatography (TLC).

General Procedure for the Synthesis of (*S*)-Indoles 12. Ts-protected aniline was dissolved in α,α,α-trifluorotoluene (0.05 M), and the mixture was cooled to −20 °C. Complex (*R*,*R*)-**S′** (5 mol %) was added, and the reaction was stirred at the same temperature for the given time. After full conversion of the starting material, the reaction was quenched by addition of 3 drops of Et_3N and concentrated. The crude was purified by flash column chromatography or preparative TLC.

Computational Methods

Calculations were performed by means of the Gaussian 09 suite of programs. DFT was applied using BP86-D3. The SDD basis set together with the corresponding Stuttgart/Dresden effective core potential was used to describe Au. The 6-31G(d) basis set was employed for all remaining atoms (H, C, N, O, F, Cl, and P). Full geometry optimizations were carried out in dichloroethane, through an implicit polarizable continuum model (PCM). The stationary points were characterized by vibrational analysis. Transition states were identified by the presence of one imaginary frequency, while minima by a full set of real frequencies. The connectivity of the transition states was confirmed by the relaxation of each transition state toward both the reactant and the product or, in some cases, by intrinsic reaction coordinate (IRC) calculations. NCIPlot was used to obtain the grid data for NCI analysis, and the corresponding results were visualized with the VMD software. Steric maps and buried volumes with spherical shape were obtained using the SambVca 2.1 web tool. The NEST web app was developed for the purpose of this study. It is available at https://besoramaria-nest-nest-01-f2n5of.streamlit.app/, and the python code can be accessed at https://github.com/BesoraMaria/NEST. NEST was used to compute the NEST occupied volume and the occupancy of the different quadrants $Q1_{occ}$, $Q2_{occ}$, $Q3_{occ}$, and $Q4_{occ}$; see details below. Geometries introduced to NEST correspond to DFT-optimized ligand-Au-Cl catalysts. Reported energies are potential energies (E) and free energies (G) in solution computed at 298.15 K and 1 atm.

All dataset collection of computational results of this manuscript is available in the ioChem-BD repository and can be accessed through https://doi.org/10.19061/iochem-bd-1-271.

ASSOCIATED CONTENT

Supporting Information

The Supporting Information is available free of charge at https://pubs.acs.org/doi/10.1021/jacsau.3c00159.

Experimental procedures, characterization data, NMR spectra, SFC and HPLC traces, DFT calculations, and crystallographic data (PDF)

NEST occupied volumes for all studied complexes (MP4)

AUTHOR INFORMATION

Corresponding Authors

Maria Besora − *Departament de Química Orgànica i Analítica, Universitat Rovira i Virgili, Tarragona 43007, Spain;* orcid.org/0000-0002-6656-5827; Email: maria.besora@urv.cat

Imma Escofet − *Institute of Chemical Research of Catalonia (ICIQ-CERCA), Barcelona Institute of Science and Technology, Tarragona 43007, Spain; Departament de Química Orgànica i Analítica, Universitat Rovira i Virgili, Tarragona 43007, Spain;* orcid.org/0000-0002-1790-4255; Email: iescofet@iciq.cat

Antonio M. Echavarren − *Institute of Chemical Research of Catalonia (ICIQ-CERCA), Barcelona Institute of Science and Technology, Tarragona 43007, Spain; Departament de Química Orgànica i Analítica, Universitat Rovira i Virgili, Tarragona 43007, Spain;* orcid.org/0000-0001-6808-3007; Email: aechavarren@iciq.es

Authors

Giuseppe Zuccarello − *Institute of Chemical Research of Catalonia (ICIQ-CERCA), Barcelona Institute of Science and Technology, Tarragona 43007, Spain*

Leonardo J. Nannini − *Institute of Chemical Research of Catalonia (ICIQ-CERCA), Barcelona Institute of Science and Technology, Tarragona 43007, Spain*

Ana Arroyo-Bondía − *Institute of Chemical Research of Catalonia (ICIQ-CERCA), Barcelona Institute of Science and Technology, Tarragona 43007, Spain; Departament de Química Orgànica i Analítica, Universitat Rovira i Virgili, Tarragona 43007, Spain*

Nicolás Fincias − *Institute of Chemical Research of Catalonia (ICIQ-CERCA), Barcelona Institute of Science and Technology, Tarragona 43007, Spain*

Isabel Arranz − *Institute of Chemical Research of Catalonia (ICIQ-CERCA), Barcelona Institute of Science and Technology, Tarragona 43007, Spain; Departament de*

Química Orgànica i Analítica, Universitat Rovira i Virgili, Tarragona 43007, Spain

Alba H. Pérez-Jimeno − *Institute of Chemical Research of Catalonia (ICIQ-CERCA), Barcelona Institute of Science and Technology, Tarragona 43007, Spain; Departament de Química Orgànica i Analítica, Universitat Rovira i Virgili, Tarragona 43007, Spain*

Matthias Peeters − *Institute of Chemical Research of Catalonia (ICIQ-CERCA), Barcelona Institute of Science and Technology, Tarragona 43007, Spain;* orcid.org/0000-0002-3445-2393

Inmaculada Martín-Torres − *Institute of Chemical Research of Catalonia (ICIQ-CERCA), Barcelona Institute of Science and Technology, Tarragona 43007, Spain*

Anna Sadurní − *Institute of Chemical Research of Catalonia (ICIQ-CERCA), Barcelona Institute of Science and Technology, Tarragona 43007, Spain*

Víctor García-Vázquez − *Institute of Chemical Research of Catalonia (ICIQ-CERCA), Barcelona Institute of Science and Technology, Tarragona 43007, Spain*

Yufei Wang − *Institute of Chemical Research of Catalonia (ICIQ-CERCA), Barcelona Institute of Science and Technology, Tarragona 43007, Spain*

Mariia S. Kirillova − *Institute of Chemical Research of Catalonia (ICIQ-CERCA), Barcelona Institute of Science and Technology, Tarragona 43007, Spain*

Marc Montesinos-Magraner − *Institute of Chemical Research of Catalonia (ICIQ-CERCA), Barcelona Institute of Science and Technology, Tarragona 43007, Spain;* orcid.org/0000-0003-1713-6257

Ulysse Caniparoli − *Institute of Chemical Research of Catalonia (ICIQ-CERCA), Barcelona Institute of Science and Technology, Tarragona 43007, Spain; Departament de Química Orgànica i Analítica, Universitat Rovira i Virgili, Tarragona 43007, Spain*

Gonzalo D. Núñez − *Departament de Química Orgànica i Analítica, Universitat Rovira i Virgili, Tarragona 43007, Spain*

Feliu Maseras − *Institute of Chemical Research of Catalonia (ICIQ-CERCA), Barcelona Institute of Science and Technology, Tarragona 43007, Spain; Departament de Química Orgànica i Analítica, Universitat Rovira i Virgili, Tarragona 43007, Spain;* orcid.org/0000-0001-8806-2019

Complete contact information is available at: https://pubs.acs.org/10.1021/jacsau.3c00159

Author Contributions

[§]G.Z., L.J.N., and A.A.-B. contributed equally. CRediT: **Giuseppe Zuccarello** investigation, writing-review & editing; **Leonardo J Nannini** investigation, writing-review & editing; **Ana Arroyo-Bondía** investigation, writing-review & editing; **Nicolas Fincias** investigation, writing-review & editing; **Isabel Arranz** investigation, writing-review & editing; **Matthias Peeters** investigation, writing-review & editing; **Inmaculada Martín-Torres** investigation, writing-review & editing; **Anna Sadurní** investigation, writing-review & editing; **Víctor García-Vázquez** investigation, writing-review & editing; **Yufei Wang** methodology, writing-review & editing; **Mariia S. Kirillova** investigation, writing-review & editing; **Marc Montesinos-Magraner** investigation, writing-review & editing; **Ulysse Caniparoli** investigation, writing-review & editing; **Gonzalo Núñez** methodology, writing-review & editing; **Feliu Maseras** methodology, writing-review & editing.

Notes

The authors declare no competing financial interest.

ACKNOWLEDGMENTS

We thank the MCIN/AEI/10.13039/501100011033 (PID2019-104815GB-I00, PID2021-128128NB-100, and CEX2019-000925-S), the European Research Council (Advanced grant 835080), the AGAUR (2021 SGR 01256), and CERCA Program/Generalitat de Catalunya for financial support. L.J.N. thanks the Swiss National Foundation (P2EZP2_181598) for an early postdoc mobility fellowship, I.A. thanks the MCIN/AEI for an FPI predoctoral fellowship, A.S. thanks the European Union (Horizon 2020 Marie Skłodowska-Curie COFUND Postdoctoral Fellowship), and M.M.-M. thanks Ministerio de Ciencia e Innovación for a Juan de la Cierva contract (IJC2019-040181-I). We also sincerely thank ICIQ X-ray diffraction, NMR, and mass spectrometry units.

REFERENCES

(1) Fürstner, A.; Davies, P. W. Catalytic Carbophilic Activation: Catalysis by Platinum and Gold π Acids. *Angew. Chem., Int. Ed.* **2007**, *46*, 3410−3449.

(2) Hashmi, A. S. K. Gold-Catalyzed Organic Reactions. *Chem. Rev.* **2007**, *38*, 3180−3211.

(3) Jiménez-Núñez, E.; Echavarren, A. M. Gold-Catalyzed Cycloisomerizations of Enynes: A Mechanistic Perspective. *Chem. Rev.* **2008**, *108*, 3326−3350.

(4) Fürstner, A. Gold and Platinum Catalysis—a Convenient Tool for Generating Molecular Complexity. *Chem. Soc. Rev.* **2009**, *38*, 3208−3221.

(5) Toste, F.; Shapiro, N. A Reactivity-Driven Approach to the Discovery and Development of Gold-Catalyzed Organic Reactions. *Synlett* **2010**, *2010*, 675−691.

(6) Obradors, C.; Echavarren, A. M. Gold-Catalyzed Rearrangements and Beyond. *Acc. Chem. Res.* **2014**, *47*, 902−912.

(7) Fensterbank, L.; Malacria, M. Molecular Complexity from Polyunsaturated Substrates: The Gold Catalysis Approach. *Acc. Chem. Res.* **2014**, *47*, 953−965.

(8) Dorel, R.; Echavarren, A. M. Gold(I)-Catalyzed Activation of Alkynes for the Construction of Molecular Complexity. *Chem. Rev.* **2015**, *115*, 9028−9072.

(9) Pflästerer, D.; Hashmi, A. S. K. Gold Catalysis in Total Synthesis - Recent Achievements. *Chem. Soc. Rev.* **2016**, *45*, 1331−1367.

(10) Chan, P.; Boyle, J.; Zhao, Y. Product Divergence in Coinage-Metal-Catalyzed Reactions of π-Rich Compounds. *Synthesis* **2018**, *50*, 1402−1416.

(11) Hashmi, A. S. K. Introduction: Gold Chemistry. *Chem. Rev.* **2021**, *121*, 8309−8310.

(12) Campeau, D.; León Rayo, D. F.; Mansour, A.; Muratov, K.; Gagosz, F. Gold-Catalyzed Reactions of Specially Activated Alkynes, Allenes, and Alkenes. *Chem. Rev.* **2021**, *121*, 8756−8867.

(13) Hashmi, A. S. K. Raising the gold standard. *Nature* **2007**, *449*, 292−293.

(14) Widenhoefer, R. A. Recent Developments in Enantioselective Gold(I) Catalysis. *Chem.—A Eur. J.* **2008**, *14*, 5382−5391.

(15) Sengupta, S.; Shi, X. Recent Advances in Asymmetric Gold Catalysis. *ChemCatChem* **2010**, *2*, 609−619.

(16) Michelet, V.; Pradal, A.; Toullec, P. Recent Developments in Asymmetric Catalysis in the Presence of Chiral Gold Complexes. *Synthesis* **2011**, *2011*, 1501−1514.

(17) Zi, W.; Dean Toste, F. Recent Advances in Enantioselective Gold Catalysis. *Chem. Soc. Rev.* **2016**, *45*, 4567−4589.

(18) Li, Y.; Li, W.; Zhang, J. Gold-Catalyzed Enantioselective Annulations. *Chem.—A Eur. J.* **2017**, *23*, 467−512.
(19) Zuccarello, G.; Zanini, M.; Echavarren, A. M. Buchwald-Type Ligands on Gold(I) Catalysis. *Isr. J. Chem.* **2020**, *60*, 360−372.
(20) Muñoz, M. P.; Adrio, J.; Carretero, J. C.; Echavarren, A. M. Ligand Effects in Gold- and Platinum-Catalyzed Cyclization of Enynes: Chiral Gold Complexes for Enantioselective Alkoxycyclization. *Organometallics* **2005**, *36*, 1293−1300.
(21) Delpont, N.; Escofet, I.; Pérez-Galán, P.; Spiegl, D.; Raducan, M.; Bour, C.; Sinisi, R.; Echavarren, A. M. Modular chiral gold(I) phosphite complexes. *Catal. Sci. Technol.* **2013**, *3*, 3007−3012.
(22) Niemeyer, Z. L.; Pindi, S.; Khrakovsky, D. A.; Kuzniewski, C. N.; Hong, C. M.; Joyce, L. A.; Sigman, M. S.; Toste, F. D. Parameterization of Acyclic Diaminocarbene Ligands Applied to a Gold(I)-Catalyzed Enantioselective Tandem Rearrangement/Cyclization. *J. Am. Chem. Soc.* **2017**, *139*, 12943−12946.
(23) Teller, H.; Flügge, S.; Goddard, R.; Fürstner, A. Enantioselective Gold Catalysis: Opportunities Provided by Monodentate Phosphoramidite Ligands with an Acyclic TADDOL Backbone. *Angew. Chem., Int. Ed.* **2010**, *49*, 1949−1953.
(24) Handa, S.; Slaughter, L. M. Enantioselective Alkynylbenzaldehyde Cyclizations Catalyzed by Chiral Gold(I) Acyclic Diaminocarbene Complexes Containing Weak Au-Arene Interactions. *Angew. Chem., Int. Ed.* **2012**, *51*, 2912−2915.
(25) Tarselli, M. A.; Chianese, A. R.; Lee, S. J.; Gagné, M. R. Gold(I)-Catalyzed Asymmetric Cycloisomerization of Eneallenes into Vinylcyclohexenes. *Angew. Chem., Int. Ed.* **2007**, *46*, 6670−6673.
(26) Franchino, A.; Martí, À.; Echavarren, A. M. H-Bonded Counterion-Directed Enantioselective Au(I) Catalysis. *J. Am. Chem. Soc.* **2022**, *144*, 3497−3509.
(27) García-Morales, C.; Ranieri, B.; Escofet, I.; López-Suarez, L.; Obradors, C.; Konovalov, A. I.; Echavarren, A. M. Enantioselective Synthesis of Cyclobutenes by Intermolecular [2+2] Cycloaddition with Non-C_2 Symmetric Digold Catalysts. *J. Am. Chem. Soc.* **2017**, *139*, 13628−13631.
(28) Li, T.; Cheng, X.; Qian, P.; Zhang, L. Gold-Catalysed Asymmetric Net Addition of Unactivated Propargylic C−H Bonds to Tethered Aldehydes. *Nat. Catal.* **2021**, *4*, 164−171.
(29) Cheng, X.; Wang, Z.; Quintanilla, C. D.; Zhang, L. Chiral Bifunctional Phosphine Ligand Enabling Gold-Catalyzed Asymmetric Isomerization of Alkyne to Allene and Asymmetric Synthesis of 2,5-Dihydrofuran. *J. Am. Chem. Soc.* **2019**, *141*, 3787−3791.
(30) Wang, Y.; Zhang, P.; Di, X.; Dai, Q.; Zhang, Z. M.; Zhang, J. Gold-Catalyzed Asymmetric Intramolecular Cyclization of N-Allenamides for the Synthesis of Chiral Tetrahydrocarbolines. *Angew. Chem., Int. Ed.* **2017**, *56*, 15905−15909.
(31) Zhang, Z. M.; Chen, P.; Li, W.; Niu, Y.; Zhao, X. L.; Zhang, J. A New Type of Chiral Sulfinamide Monophosphine Ligands: Stereodivergent Synthesis and Application in Enantioselective Gold(I)-Catalyzed Cycloaddition Reactions. *Angew. Chem., Int. Ed.* **2014**, *53*, 4350−4354.
(32) Zhang, Z.; Smal, V.; Retailleau, P.; Voituriez, A.; Frison, G.; Marinetti, A.; Guinchard, X. Tethered Counterion-Directed Catalysis: Merging the Chiral Ion-Pairing and Bifunctional Ligand Strategies in Enantioselective Gold(I) Catalysis. *J. Am. Chem. Soc.* **2020**, *142*, 3797−3805.
(33) Bohan, P. T.; Toste, F. D. Well-Defined Chiral Gold(III) Complex Catalyzed Direct Enantioconvergent Kinetic Resolution of 1,5-Enynes. *J. Am. Chem. Soc.* **2017**, *139*, 11016−11019.
(34) Reid, J. P.; Hu, M.; Ito, S.; Huang, B.; Hong, C. M.; Xiang, H.; Sigman, M. S.; Toste, F. D. Strategies for Remote Enantiocontrol in Chiral Gold(III) Complexes Applied to Catalytic Enantioselective γ,δ-Diels-Alder Reactions. *Chem. Sci.* **2020**, *11*, 6450−6456.
(35) Martín-Torres, I.; Ogalla, G.; Yang, J. M.; Rinaldi, A.; Echavarren, A. M. Enantioselective Alkoxycyclization of 1,6-Enynes with Gold(I)-Cavitands: Total Synthesis of Mafaicheenamine C. *Angew. Chem., Int. Ed.* **2021**, *60*, 9339−9344.
(36) Zuccarello, G.; Mayans, J. G.; Escofet, I.; Scharnagel, D.; Kirillova, M. S.; Pérez-Jimeno, A. H.; Calleja, P.; Boothe, J. R.; Echavarren, A. M. Enantioselective Folding of Enynes by Gold(I) Catalysts with a Remote C_2-Chiral Element. *J. Am. Chem. Soc.* **2019**, *141*, 11858−11863.
(37) Nieto-Oberhuber, C.; López, S.; Echavarren, A. M. Intramolecular [4+2] Cycloadditions of 1,3-Enynes or Arylalkynes with Alkenes with Highly Reactive Cationic Phosphine Au(I) Complexes. *J. Am. Chem. Soc.* **2005**, *127*, 6178−6179.
(38) Nieto-Oberhuber, C.; Pérez-Galán, P.; Herrero-Gómez, E.; Lauterbach, T.; Rodríguez, C.; López, S.; Bour, C.; Rosellón, A.; Cárdenas, D. J.; Echavarren, A. M. Gold(I)-Catalyzed Intramolecular [4+2] Cycloadditions of Arylalkynes or 1,3-Enynes with Alkenes: Scope and Mechanism. *J. Am. Chem. Soc.* **2008**, *130*, 269−279.
(39) Caniparoli, U.; Escofet, I.; Echavarren, A. M. Planar Chiral 1,3-Disubstituted Ferrocenyl Phosphine Gold(I) Catalysts. *ACS Catal.* **2022**, *12*, 3317−3322.
(40) See Supporting Information for details. A dataset collection of computational results is available in the ioChem-BD repository and can be accessed https://iochem-bd.iciq.es/browse/handle/100/59809 Álvarez-Moreno, M.; De Graaf, C.; López, N.; Maseras, F.; Poblet, J. M.; Bo, C. Managing the Computational Chemistry Big Data Problem: The ioChem-BD Platform. *J. Chem. Inf. Model.* **2015**, *55*, 95−103.
(41) (a) Francos, J.; Grande-Carmona, F.; Faustino, H.; Iglesias-Sigüenza, J.; Díez, E.; Alonso, I.; Fernández, R.; Lassaletta, J. M.; López, F.; Mascareñas, J. L. Axially Chiral Triazoloisoquinolin-3-Ylidene Ligands in Gold(I)-Catalyzed Asymmetric Intermolecular (4 + 2) Cycloadditions of Allenamides and Dienes. *J. Am. Chem. Soc.* **2012**, *134*, 14322−14325. (b) Varela, I.; Faustino, H.; Díez, E.; Iglesias-Sigüenza, J.; Grande-Carmona, F.; Fernández, R.; Lassaletta, J. M.; Mascareñas, J. L.; López, F. Gold(I)-Catalyzed Enantioselective [2+2+2] Cycloadditions: An Expedient Entry to Enantioenriched Tetrahydropyran Scaffolds. *ACS Catal.* **2017**, *7*, 2397−2402.
(42) Mailig, M.; Rucker, R. P.; Lalic, G. Practical catalytic method for synthesis of sterically hindered anilines. *Chem. Commun.* **2015**, *51*, 11048−11051.
(43) Navarro, M.; Miranda-Pizarro, J.; Moreno, J. J.; Navarro-Gilabert, C.; Fernández, I.; Campos, J. A dicoordinate gold(i)−ethylene complex. *Chem. Commun.* **2021**, *57*, 9280−9283.
(44) Navarro, M.; Alférez, M. G.; de Sousa, M.; Miranda-Pizarro, J.; Campos, J. Dicoordinate Au(I)−Ethylene Complexes as Hydroamination Catalysts. *ACS Catal.* **2022**, *12*, 4227−4241.
(45) Muratov, K.; Gagosz, F. Confinement-Induced Selectivities in Gold(I) Catalysis—The Benefit of Using Bulky Tri-(ortho-biaryl)-Phosphine Ligands. *Angew. Chem., Int. Ed.* **2022**, *61*, No. e202203452.
(46) Yoon, T. P.; Jacobsen, E. N. Privileged Chiral Catalysts. *Science* **2003**, *299*, 1691−1693.
(47) Chen, Y.; Yekta, S.; Yudin, A. K. Modified BINOL Ligands in Asymmetric Catalysis. *Chem. Rev.* **2003**, *103*, 3155−3212.
(48) Brunel, J. M. BINOL: A Versatile Chiral Reagent. *Chem. Rev.* **2005**, *105*, 857−898.
(49) Maji, R.; Mallojjala, S. C.; Wheeler, S. E. Chiral phosphoric acid catalysis: from numbers to insights. *Chem. Soc. Rev.* **2018**, *47*, 1142−1158.
(50) Parmar, D.; Sugiono, E.; Raja, S.; Rueping, M. Complete Field Guide to Asymmetric BINOL-Phosphate Derived Brønsted Acid and Metal Catalysis: History and Classification by Mode of Activation; Brønsted Acidity, Hydrogen Bonding, Ion Pairing, and Metal Phosphates. *Chem. Rev.* **2014**, *114*, 9047−9153.
(51) Čorić, I.; List, B. Asymmetric spiroacetalization catalysed by confined Brønsted acids. *Nature* **2012**, *483*, 315−319.
(52) Bringmann, G.; Price Mortimer, A. J.; Keller, P. A.; Gresser, M. J.; Garner, J.; Breuning, M. Atroposelective Synthesis of Axially Chiral Biaryl Compounds. *Angew. Chem., Int. Ed.* **2005**, *44*, 5384−5427.
(53) Clayden, J.; Moran, W. J.; Edwards, P. J.; Laplante, S. R. The Challenge of Atropisomerism in Drug Discovery. *Angew. Chem., Int. Ed.* **2009**, *48*, 6398−6401.
(54) Laplante, S. R.; Edwards, P. J.; Fader, L. D.; Jakalian, A.; Hucke, O. Revealing Atropisomer Axial Chirality in Drug Discovery. *ChemMedChem* **2011**, *6*, 505−513.

https://doi.org/10.1021/jacsau.3c00159
JACS Au 2023, 3, 1742−1754

(55) Laplante, S. R.; Fader, L. D.; Fandrick, K. R.; Fandrick, D. R.; Hucke, O.; Kemper, R.; Miller, S. P. F.; Edwards, P. J. Assessing Atropisomer Axial Chirality in Drug Discovery and Development. *J. Med. Chem.* **2011**, *54*, 7005−7022.
(56) Kozlowski, M. C.; Morgan, B. J.; Linton, E. C. Total synthesis of chiral biaryl natural products by asymmetric biaryl coupling. *Chem. Soc. Rev.* **2009**, *38*, 3193−3207.
(57) Bringmann, G.; Gulder, T.; Gulder, T. A. M.; Breuning, M. Atroposelective Total Synthesis of Axially Chiral Biaryl Natural Products. *Chem. Rev.* **2011**, *111*, 563−639.
(58) Pu, L. 1,1'-Binaphthyl Dimers, Oligomers, and Polymers: Molecular Recognition, Asymmetric Catalysis, and New Materials. *Chem. Rev.* **1998**, *98*, 2405−2494.
(59) Pu, L. Enantioselective Fluorescent Sensors: A Tale of BINOL. *Acc. Chem. Res.* **2012**, *45*, 150−163.
(60) Cheng, J. K.; Xiang, S.; Li, S.; Ye, L.; Tan, B. Recent Advances in Catalytic Asymmetric Construction of Atropisomers. *Chem. Rev.* **2021**, *121*, 4805−4902.
(61) Bringmann, G.; Price Mortimer, A. J.; Keller, P. A.; Gresser, M. J.; Garner, J.; Breuning, M. Atroposelective Synthesis of Axially Chiral Biaryl Compounds. *Angew. Chem., Int. Ed.* **2005**, *44*, 5384−5427.
(62) Zhang, J.; Simon, M.; Golz, C.; Alcarazo, M. Gold-Catalyzed Atroposelective Synthesis of 1,1′-Binaphthalene-2,3′-diols. *Angew. Chem., Int. Ed.* **2020**, *59*, 5647−5650.
(63) Li, T. Z.; Liu, S. J.; Tan, W.; Shi, F. Catalytic Asymmetric Construction of Axially Chiral Indole-Based Frameworks: An Emerging Area. *Chem.—Eur. J.* **2020**, *26*, 15779−15792.
(64) Peng, L.; Li, K.; Xie, C.; Li, S.; Xu, D.; Qin, W.; Yan, H. Organocatalytic Asymmetric Annulation of ortho-Alkynylanilines: Synthesis of Axially Chiral Naphthyl-C2-indoles. *Angew. Chem., Int. Ed.* **2019**, *58*, 17199−17204.
(65) He, Y. P.; Wu, H.; Wang, Q.; Zhu, J. Palladium-Catalyzed Enantioselective Cacchi Reaction: Asymmetric Synthesis of Axially Chiral 2,3-Disubstituted Indoles. *Angew. Chem., Int. Ed.* **2020**, *59*, 2105−2109.
(66) Yu, L.; Liu, J.; Xiang, S.; Lu, T.; Ma, P.; Zhao, Q. Silver-Catalyzed Direct Nucleophilic Cyclization: Enantioselective De Novo Synthesis of C−C Axially Chiral 2-Arylindoles. *Org. Lett.* **2023**, *25*, 522−527.
(67) Johnson, E. R.; Keinan, S.; Mori-Sánchez, P.; Contreras-García, J.; Cohen, A. J.; Yang, W. Revealing Noncovalent Interactions. *J. Am. Chem. Soc.* **2010**, *132*, 6498−6506.
(68) Contreras-García, J.; Johnson, E. R.; Keinan, S.; Chaudret, R.; Piquemal, J.-P.; Beratan, D. N.; Yang, W. NCIPLOT: A Program for Plotting Noncovalent Interaction Regions. *J. Chem. Theory Comput.* **2011**, *7*, 625−632.
(69) Ribas, J.; Cubero, E.; Luque, F. J.; Orozco, M. J. Theoretical Study of Alkyl-π and Aryl-π Interactions. Reconciling Theory and Experiment. *Org. Chem.* **2002**, *67*, 7057−7065.
(70) Ninković, D. B.; Vojislavljević-Vasilev, D. Z.; Medaković, V. B.; Hall, M. B.; Brothers, E. N.; Zarić, S. D. Aliphatic−aromatic stacking interactions in cyclohexane−benzene are stronger than aromatic−aromatic interaction in the benzene dimer. *Phys. Chem. Chem. Phys.* **2016**, *18*, 25791−25795.
(71) Ninković, D. B.; Blagojević-Filipović, J. P.; Hall, M. B.; Brothers, E. N.; Zarić, S. D. What Is Special about Aromatic−Aromatic Interactions? Significant Attraction at Large Horizontal Displacement. *ACS Cent. Sci.* **2020**, *6*, 420−425.
(72) Pracht, P.; Bohle, F.; Grimme, S. Automated exploration of the low-energy chemical space with fast quantum chemical methods. *Phys. Chem. Chem. Phys.* **2020**, *22*, 7169−7192.
(73) Clavier, H.; Nolan, S. P. Percent buried volume for phosphine and N-heterocyclic carbeneligands: steric properties in organometallic chemistry. *Chem. Commun.* **2010**, *46*, 841−861.
(74) Falivene, L.; Cao, Z.; Petta, A.; Serra, L.; Poater, A.; Oliva, R.; Scarano, V.; Cavallo, L. Towards the online computer-aided design of catalytic pockets. *Nat. Chem.* **2019**, *11*, 872−879.
(75) Pizarro, J. D.; Molina, F.; Fructos, M. R.; Pérez, P. J. Gold Complexes with ADAP Ligands: Effect of Bulkiness in Catalytic Carbene Transfer Reactions (ADAP = Alkoxydiaminophosphine). *Organometallics* **2020**, *39*, 2553−2559.
(76) Ruch, A. A.; Ellison, M. C.; Nguyen, J. K.; Kong, F.; Handa, S.; Nesterov, V. N.; Slaughter, L. M. Highly Sterically Encumbered Gold Acyclic Diaminocarbene Complexes: Overriding Electronic Control in Regiodivergent Gold Catalysis. *Organometallics* **2021**, *40*, 1416−1433.
(77) Aguado-Ullate, S.; Saureu, S.; Guasch, L.; Carbó, J. J. Theoretical Studies of Asymmetric Hydroformylation Using the Rh-(R,S)-BINAPHOS Catalyst—Origin of Coordination Preferences and Stereoinduction. *Chem.—Eur. J.* **2012**, *18*, 995−1005.
(78) Aguado-Ullate, S.; Urbano-Cuadrado, M.; Villalba, I.; Pires, E.; García, J. I.; Bo, C.; Carbó, J. J. Predicting the Enantioselectivity of the Copper-Catalysed Cyclopropanation of Alkenes by Using Quantitative Quadrant-Diagram Representations of the Catalysts. *Chem.—Eur. J.* **2012**, *18*, 14026−14036.
(79) Besora, M.; Olmos, A.; Gava, R.; Noverges, B.; Asensio, G.; Caballero, A.; Maseras, F.; Pérez, P. J. A Quantitative Model for Alkane Nucleophilicity Based on C−H Bond Structural/Topological Descriptors. *Angew. Chem., Int. Ed.* **2020**, *59*, 3112−3116.
(80) Lakuntza, O.; Besora, M.; Maseras, F. Searching for Hidden Descriptors in the Metal−Ligand Bond through Statistical Analysis of Density Functional Theory (DFT) Results. *Inorg. Chem.* **2018**, *57*, 14660−14670.
(81) For the cyclization of 1b, the NEST model was built with catalysts A, A', F', G, X, and Y and was predicted for B, H, J, L, M, N, S-U, and W. For the cyclization of 1a, the NEST model was built with catalysts A, B, G, H, L-N, S-U, and W and was predicted for A', F', J, X, and Y. For the cyclization of 11a, the NEST model was built with catalysts A, A'', B, F', G, J, L-N, S-U, and W and was predicted for F', X, H, and Y.

https://doi.org/10.1021/jacsau.3c00159
JACS Au 2023, 3, 1742−1754